NASA Technical Memorandum 86029

NASA-TM-86029 19840024314

Air Data Position-Error Calibration Using State Reconstruction Techniques

Stephen A. Whitmore, Terry J. Larson, and L. J. Ehernberger

September 1984

National Aeronautics and
Space Administration

NASA Technical Memorandum 86029

Air Data Position-Error Calibration Using State Reconstruction Techniques

Stephen A. Whitmore, Terry J. Larson, and L. J. Ehernberger
NASA Ames Research Center, Dryden Flight Research Facility, Edwards, California 93523

1984

National Aeronautics and
Space Administration
Ames Research Center
Dryden Flight Research Facility
Edwards, California 93523

SUMMARY

During the highly maneuverable aircraft technology (HiMAT) flight test program recently completed at NASA Ames Research Center's Dryden Flight Research Facility, numerous problems were experienced in airspeed calibration. This necessitated the use of state reconstruction techniques to arrive at a position-error calibration. For the HiMAT aircraft, most of the calibration effort was expended on flights in which the air data pressure transducers were not performing accurately. Following discovery of this problem, the air data transducers of both aircraft were wrapped in heater blankets to correct the problem. Additional calibration flights were performed, and from the resulting data a satisfactory position-error calibration was obtained.

This calibration and data obtained before installation of the heater blankets were used to develop an alternate calibration method. The alternate approach took advantage of high-quality inertial data that was readily available. A linearized Kalman filter (LKF) was used to reconstruct the aircraft's wind-relative trajectory; the trajectory was then used to separate transducer measurement errors from the aircraft position error. As a result, a calibration that was corrected for transducer measurement error was obtained. The data were investigated for accuracy through statistical techniques by comparison to the data from the pace aircraft, and by comparison to the position-error curve resulting from the data obtained after the installation of the heater blankets. The results are presented in this paper.

This calibration method is accurate and inexpensive. The LKF technique has an inherent advantage of requiring that no flight maneuvers be specially designed for airspeed calibrations. It is of particular use when the measurements of the wind-relative quantities are suspected to have transducer-related errors.

INTRODUCTION

Air data parameters, such as airspeed, Mach number, angle of attack, and impact pressure, describe most of an aircraft's wind-relative dynamics. Accurate estimates of their values are essential for analyses such as performance assessment and stability and control derivative extraction. The standard air data method uses pneumatic measurements (ref. 1) that are strongly influenced by the presence of the aircraft fuselage. This fuselage effect is commonly referred to as aircraft position error, and must be accounted for by an independent calibration of the measurement system under the exact conditions that are to be experienced in flight (ref. 2).

For the highly maneuverable aircraft technology (HiMAT) flight test program completed recently at NASA Ames Research Center's Dryden Flight Research Facility, most of the calibration data were obtained during flights in which the air data pressure transducers were not performing accurately. During early calibration flights, the static (ambient) and impact pressure measurements showed sizable, nonrepeatable deviations from the values predicted by wind tunnel data. The deviations were suspected to be caused by the exposure of the air data transducers to temperatures outside of the prescribed temperature operating range. To solve the problem, the air data transducers were removed, wrapped in heater blankets, and reinstalled. Additional calibration flights were performed and a satisfactory position-error calibration was obtained.

The data obtained before the installation of the heater blankets provided a set of experimental data with which advanced calibration techniques could be developed. Using that data set, the goal was to develop an accurate technique allowing for the separation of transducer measurement errors from the aircraft position error. The technique took advantage of high-quality inertial measurements that were readily available. Once this technique was developed, a corrected position-error calibration was computed. Because of prior knowledge that transducer measurement errors are mostly the result of random temperature effects, the calibration resulting from the advanced technique could either be verified or contradicted by comparison to the calibration data obtained after the installation of the heater blankets.

The technique presented in this paper uses a linearized Kalman filter (LKF) to reconstruct the aircraft's wind-relative trajectory. Data obtained from a single flight performed before the installation of the transducer heater blankets was used. The reconstruction was performed so that resulting estimates are only slightly dependent on both aircraft position error and transducer measurement error. This allowed for identification of transducer error trends and the approximate separation of transducer measurement error from aircraft position error. Using these transducer error estimates, the indicated air data measurements were corrected; a position-error calibration was then computed. The LKF technique has the advantage of requiring that no flight maneuvers be specially designed for airspeed calibrations. It can use either steady-state or dynamic data, and can separate transducer measurement error from actual aircraft position errors. It has the flexibility to accommodate a variety of different data sources. The LKF technique is of particular use when the measurements of the wind-relative quantities are suspected to be of poor quality. In that case, the complementary information provided by alternate, readily available sources (to be discussed in the DATA SOURCES AND INSTRUMENTATION section) still allows for a reasonable calibration. The resulting calibration is of comparable accuracy when compared with calibrations resulting from traditional means.

NOMENCLATURE

A	stability matrix
ax, ay, an	aircraft body-axis linear accelerations (longitudinal, lateral, normal), m/sec^2 (ft/sec^2)
B	control matrix
C	measurement equation matrix
e	innovations vector
F	state noise gain matrix
FF	covariance of state noise sequence
FIR	finite impulse response
G	measurement noise gain matrix
GG	covariance of measurement noise sequence

GMT	Greenwich mean time
g	acceleration of gravity at sea level, m/sec^2 (ft/sec^2)
H	geometric altitude, m (ft)
HiMAT	highly maneuverable aircraft technology
Hp	pressure altitude, m (ft)
I	identity matrix
j	summation index
K	Kalman gain matrix
k	discrete time sample number
LKF	linearized Kalman filter
M	true Mach number
M_i	indicated Mach number
ND	number of points used in computing the sample mean of the innovations components
P	static pressure, N/m^2 (lb/ft^2)
Q	filter error covariance
Qc	impact pressure N/m^2 (lb/ft^2)
RPRV	remotely piloted research vehicle
T	temperature, °C (°F)
Ts	sample interval of discrete measurements, sec
t	time, sec
U	state equation input vector
V	total Earth relative velocity
Vew, Vns, Vv	Earth-relative velocity components with respect to topodetic axis system (fixed at Edwards AFB) in the northerly, easterly, and vertical directions (positive downward), m/sec (ft/sec)
VW	total airspeed
VWew, VWns, VWv	airspeed components with respect to topodetic axis system (fixed at Edwards AFB) in the northerly, easterly, and vertical directions (positive downward), m/sec (ft/sec)

W	total windspeed
Wew, Wns, Wv	windspeed components with respect to topodetic axis system, with the components blowing from the northerly, easterly, and vertical directions (positive upward), m/sec (ft/sec)
x	state vector
Z	vector of known pressure measurements
z	measurement vector
ΔM	$M - M_i$
η	zero mean, unit covariance, Gaussian distributed, time varying random sequence
θ	pitch angle, deg
ρ	error vector
Φ	state transition matrix
ϕ	bank angle, deg
Ψ	input transition matrix
ψ	heading angle, deg

Mathematical operators and special symbols:

DET	determinate of quantity
d/dt( )	derivative of ( ) with respect to time
S( )	sample mean of the quantity ( )
δ( )	error in quantity ( ) due to transducer
Δ( )	error in quantity ( ) due to position error

Superscripts:

T	matrix transpose
-1	matrix inverse

Subscripts:

backup	backup transducer quantity
c	quantity corrected for transducer error
f	quantity estimated by LKF analysis

main	main transducer quantity
true	exact value of quantity

DESCRIPTION OF HiMAT AIRCRAFT

The HiMAT aircraft is a highly maneuverable, remotely piloted, subscale vehicle flown at NASA Ames Research Center's Dryden Flight Research Facility from 1979 to 1983. It is a 0.44-scale version of an envisioned full-scale aircraft and has a maneuverability goal of a sustained 8g turn at Mach 0.90 and at an altitude of 7620 m (25,000 ft). A J85-21 engine with afterburner capability provides propulsion for the HiMAT aircraft. The vehicle features high-technology innovations such as a close-coupled canard, relaxed static stability, and composite structural materials. Figure 1(a) is a photograph of the HiMAT vehicle; the remotely piloted vehicle concept is illustrated in figure 1(b).

Closed-loop primary flight control is performed from a ground-based cockpit and a digital computer in conjunction with an uplink/downlink telemetry system. In addition to the uplink/downlink system, the HiMAT aircraft is fully instrumented with a high-quality, research-oriented data acquisition system. This system features onboard data recording and ground-based, postflight processing of data. Many of the onboard measurement sensors are used for both research data acquisition and feedback signals in the uplink/downlink control system (ref. 3).

DATA SOURCES AND INSTRUMENTATION

The linearized Kalman filter (LKF) technique uses several data sources to compute the wind-relative trajectory estimates. These sources are: air data measurements provided by a conventional nose-mounted pitot-static system, ground-based radar resulting from the uplink/downlink tracking, steady-state meteorological and barometric conditions derived from weather charts and balloon data, and measurements of aircraft inertial accelerations and rotation rate data from onboard sensors. These data sources are all available as part of the nominal flight operations. None of the data sources, used alone, provide enough information to arrive at a sufficiently accurate answer; however, when combined, they sometimes provide information beyond that which is needed to attain highly accurate trajectory estimates. A discussion of each of these data sources follows.

HiMAT Air Data Measurements

The HiMAT air data are measured by a nose-mounted probe that is a 0.50-scale version of the NACA-designed pitot-static probe (ref. 4). The air data pressures are sensed by main and backup sets of variable-capacitance absolute and differential transducers. The static transducers, both main and backup, are fed by the same static pressure source. The impact transducers (both main and backup) are fed by a single-stagnation pressure source and by the static pressure source; the impact transducers measure the differences between stagnation and impact pressure sources. Figure 2(a) illustrates the noseboom as it is mounted on the HiMAT aircraft and

figure 2(b) is a schematic of the air data sensor system. When the temperature-operating range of 35° to 70° C is not exceeded, the manufacturer's expected accuracies for both types of transducers is 0.1 percent of full-scale reading. Outside of the operating range, the expected accuracy is 0.1 percent ±0.2 percent per degree, C. Because the backup transducers exhibited less sensitivity to temperature overranges, the data resulting from backup transducers were used for the trajectory reconstruction.

Angles of attack and sideslip are measured by flow-direction vanes incorporated into the nose-mounted pitot-static probe. Resulting flow-angle deflections are corrected for fuselage upwash and pitch, roll, and yaw rates. Calibrated values are typically accurate to within 0.5° under stabilized flight conditions.

Radar Measurements

The radar values were obtained from a beacon track on the aircraft using the Ames Dryden FPS-16 radar facility (ref. 5). The resulting time histories of range, elevation angle, and azimuth angle were converted to position and differentiated to give Earth-relative velocity in the northerly, easterly, and vertical (positive downward) directions. Under nominal conditions the Ames Dryden FPS-16 radar facility is believed to be accurate to within 5 m (15 ft) in range and 0.001° in azimuth and elevation angles.

Meteorological Measurements

The analysis of meteorological conditions employed upper-air charts produced by the National Meteorological Center at 1200 hr Greenwich Mean Time (GMT) for the day before the flight and at 00 hr GMT on the day following the flight. Individual rawinsound (radar and wind and radiosonde) balloon observations from nearby stations were used to chart conditions at additional levels in the atmosphere, and to examine the detailed vertical structure of the atmosphere. Values of pressure altitude, temperature, wind direction, and windspeed were interpolated to give estimates for the flight test location and time as a function of geometric altitude. Accuracies of the meteorological data are dependent on weather conditions prevailing at the time in which the measurements are recorded. An in-depth discussion of the accuracies is in the VALIDATION OF THE LKF TECHNIQUES section.

Onboard Inertial Measurements

The onboard instrumentation system has two sets of good resolution, high accuracy, strapdown linear accelerometers. The manufacturer's expected accuracy of these accelerometers is 0.05 percent of full scale, and the expected resolution is 0.01 percent of full scale. Acceleration time histories about the aircraft's normal, lateral, and longitudinal axes are recorded. The two measurement sets are corrected for offset from the aircraft's center of gravity by using measured values of pitch, roll, and yaw rates. The values of pitch, roll, and yaw rates are measured by a strapdown-rate gyro package with accuracy and resolution similar to that of the accelerometer package. The Euler angles are measured by a gimballed, stabilized inertial platform. Manufacturer's expected accuracies for the platform are 0.2° random accuracy in all three axes and a drift rate of 1 deg/hr in heading after the stabilization of the platform.

ANALYSIS

As previously mentioned, the goal of this analysis was to develop and verify an advanced technique that could be used to perform accurate air data calibrations, using commonly available data sources, without requiring specially designed flight maneuvers and procedures. To assure greater accuracy in the calibration, the technique should provide some means for separating transducer measurement errors from aircraft position error. Data from a single HiMAT flight performed before the installation of heater blankets was used to develop and test the technique, and the calibration data obtained after the installation of the heater blankets was used to evaluate the results. A brief summary of how position-error calibrations are performed and the problems which were encountered with the HiMAT calibration is presented.

Summary of Traditional Position-Error Calibration Techniques

Position error is a strong function of Mach number and is often presented in terms of a Mach calibration curve. The curve is the difference between true and indicated Mach numbers (M and M_i, respectively) crossplotted against the indicated Mach number. Indicated Mach number refers to the Mach number computed from the air data transducer pressure measurements (static and impact) in the absence of any kind of position-error correction. The true Mach number is usually computed or measured by an independent source such as a pace aircraft or radar tracking. The position-error, ΔM, as described by the position-error curve, is added to the indicated Mach number (as a function of the indicated Mach number) to arrive at an estimate of true Mach number.

This calibration technique assumes that there are no errors in the transducer pressure measurements (that is, that the only error source is the error caused by the interference of the ambient field by the aircraft configuration). The M curve almost always takes on a characteristic shape; any scatter or deviation from this shape is indicative of errors in the original calibration data. Scatter of this type reduces the confidence placed in the accuracy of the calibration curve. This is a recurrent problem in airspeed calibration; a method of separating the transducer errors from the actual position error is highly desirable.

Error Sources for HiMAT Transducers

The early HiMAT calibration efforts were subject to the scatter problem previously mentioned. Figure 3 presents the position-error data (recorded from the main transducer) that were obtained during HiMAT vehicle flights performed before the installation of the transducer heater blankets. Also presented is the position-error curve data obtained from testing in the 11- by 11-Foot Transonic Wind Tunnel at NASA Ames Research Center, Moffett Field, California. The flight calibration data lie well above the wind tunnel curve. This disagreement, combined with the uncharacteristically shallow slope of the flight data, led to the assumption that the transducer measurements were in error.

To determine if the measurements were in error, both sets of transducers were removed from the aircraft and taken to the calibration laboratory where they were checked for temperature sensitivity. All of the transducers were shown to experience random temperature-related errors. In the laboratory, the temperature

deviations appeared when the transducers were exposed to temperatures of less than 7° C. From onboard thermocouple measurements it was determined that the transducers unexpectedly experienced temperatures below 7° C during nominal flight conditions. Those temperatures were outside of the manufacturer's recommended operating range.

As a corrective action, all transducers were wrapped in heater blankets and reinstalled. Three flights were then performed and new calibration data were obtained. These data are presented, along with the wind tunnel curve, in figure 4. The data are in good agreement and the calibration is considered to be sufficiently accurate for both operational and analysis purposes.

Description of the Estimation Algorithm

In the analysis to be developed in this paper, the true Mach number required to compute the position-error calibration curve (as previously described) is estimated by combining the inertial, radar, pneumatic, and meteorological data with a linearized Kalman filter. The Kalman filter gives the optimal estimate for the state of any linear system in which Gaussian statistics occur (refs. 6, 7, and 8). The dynamics of the system are modeled by a matrix differential equation of the form:

$$d/dt[x(t)] = A(t)x(t) + B(t)U(t) + F\eta(t) \tag{1a}$$

$$z(t) = C(t)x(t) + G\eta(t) \tag{1b}$$

where the vector $x(t)$ represents the state of the system and is to be estimated; $U(t)$ represents determined inputs to the system; and $z(t)$ represents the system's outputs. These outputs may be directly measured, and are referred to as system measurements. The additive terms $F\eta(t)$ and $G\eta(t)$, are zero mean, Gaussian white noise sequences with covariances FF and GG. The sequence, $F\eta(t)$ is referred to as the state noise; $G\eta(t)$ is referred to as measurement noise. The state noise is a stochastic disturbance of the system's dynamics. The measurement noise is the random error in the measurements of the system's response. Equation (1a) is referred to as the state equation, and equation (1b) is referred to as the measurement equation.

The discrete form of the Kalman filter is used for this analysis, so the system equations presented must be discretized. The continuous time-state equation is discretized via Euler integration (the filter is referred to as a linearized Kalman filter for this reason) and the measurement equation is discretized by inspection. The Kalman filter is then directly applied to the resulting difference equations. The system discretization and the discrete-time Kalman filter equations are presented in appendix A.

The algorithm consists of a prediction and a correction step. The prediction step extrapolates the current state to the next time point. This result is referred to as the predicted state. The correction step uses the predicted state, along with the measurement vector corresponding to the next time point, to compute an updated state estimate. This estimate is the optimal filtered state at sample $k + 1$ and is based on $k + 2$ measurements — that is, the updated estimate at time $k + 1$ has been computed based on information taken from the measurement sequence $z(0)$, $z(1)$, . . . $z(k + 1)$. The filter is recursive — that is, at each iteration the filter depends only on the last state estimate and the current measurement, and is implemented for successive data frames until the measurement time histories have been exhausted.

System Equations

For this analysis, the state equation (that is, the expansion of equation (1a) is

$$\frac{d}{dt}\begin{bmatrix} Vns \\ Vew \\ Vv \\ Wns \\ Wew \\ Wv \\ H \end{bmatrix} = \begin{bmatrix} 0 & 0 & 0 & 0 & 0 & 0 & 0 \\ 0 & 0 & 0 & 0 & 0 & 0 & 0 \\ 0 & 0 & 0 & 0 & 0 & 0 & 0 \\ 0 & 0 & 0 & 0 & 0 & 0 & 0 \\ 0 & 0 & 0 & 0 & 0 & 0 & 0 \\ 0 & 0 & 0 & 0 & 0 & 0 & 0 \\ 0 & 0 & -1 & 0 & 0 & 0 & 0 \end{bmatrix} \begin{bmatrix} Vns \\ Vew \\ Vv \\ Wns \\ Wew \\ Wv \\ H \end{bmatrix} + \begin{bmatrix} & & & 0 \\ & f(\theta, \phi, \psi) & & 0 \\ & & & -1 \\ 0 & 0 & 0 & 0 \\ 0 & 0 & 0 & 0 \\ 0 & 0 & 0 & 0 \\ 0 & 0 & 0 & 0 \end{bmatrix} \begin{bmatrix} ax \\ ay \\ an \\ g \end{bmatrix} + F\eta(t) \qquad (2a)$$

and the measurement equation (that is, the expansion of equation (1b)) is

$$\begin{bmatrix} Vns \\ Vew \\ Vv \\ VWns \\ VWew \\ VWv \\ Wns \\ Wew \\ Wv \\ H \end{bmatrix} = \begin{bmatrix} 1 & 0 & 0 & 0 & 0 & 0 & 0 \\ 0 & 1 & 0 & 0 & 0 & 0 & 0 \\ 0 & 0 & 1 & 0 & 0 & 0 & 0 \\ 1 & 0 & 0 & 1 & 0 & 0 & 0 \\ 0 & 1 & 0 & 0 & 1 & 0 & 0 \\ 0 & 0 & 1 & 0 & 0 & 1 & 0 \\ 0 & 0 & 0 & 1 & 0 & 0 & 0 \\ 0 & 0 & 0 & 0 & 1 & 0 & 0 \\ 0 & 0 & 0 & 0 & 0 & 1 & 0 \\ 0 & 0 & 0 & 0 & 0 & 0 & 1 \end{bmatrix} \begin{bmatrix} Vns \\ Vew \\ Vv \\ Wns \\ Wew \\ Wv \\ H \end{bmatrix} + G\eta(t) \qquad (2b)$$

The partitioned submatrix $f(\theta, \phi, \psi)$ is the 3 by 3 direction cosine matrix that describes the transformation from the aircraft body axis coordinates to topodetic (locally level) coordinates (ref. 9). This matrix is

$$f(\theta, \phi, \psi) = \begin{bmatrix} \cos\phi & \sin\phi & 0 \\ -\sin\phi & \cos\phi & 0 \\ 0 & 0 & 1 \end{bmatrix} \begin{bmatrix} 1 & 0 & 0 \\ 0 & \cos\psi & \sin\psi \\ 0 & -\sin\psi & \cos\psi \end{bmatrix} \begin{bmatrix} \cos\theta & 0 & -\sin\theta \\ 0 & 1 & 0 \\ \sin\theta & 0 & \cos\theta \end{bmatrix}$$

It is shown in equations (1a) and (2a) that the state equation is seventh-order and includes only one feedback term, the relationship between altitude (H) and vertical velocity. The wind dynamics are assumed to be driven by random walk. The seven elements of the state vector are the Earth-relative velocity components in the northerly, easterly, and vertical directions, where the vertical velocity is defined to be positive downward; the wind velocity components from the northerly, easterly, and vertical directions (positive upward); and geometric altitude.

It is also shown in equations (1a) and (2a) that there are four inputs to the state equation. The first three inputs are the previously described strapdown body-axis acceleration measurements and the fourth is the acceleration of gravity as a function of altitude (expressed in topodetic coordinates).

In equations (1b) and (2b), the measurement vector has ten elements and consists of the measured radar velocity components, the wind-relative airspeed components (from the backup transducer), the meteorologic estimates for the wind components, and the radar altitude. All of these quantities are expressed in topodetic coordinates. The measurements are related to the state estimates via the measurement geometry matrix, C.

Measurement Weightings

As previously described, the measurement equation is assumed to be corrupted by zero mean, Gaussian white noise that has a covariance of GG. The GG matrix is an inverse matrix; that is, the reciprocals of the diagonal elements of GG are used to weight the individual elements of the z(t) vector, which allows for selective filtering of information from the measured values. Measurements with small covariances (large weightings) will have very little information filtered out of them. On the other hand, measurements with large covariances (low weightings) will be heavily filtered. The selection of these weightings is an important part of the analysis and allows the user to shape the filter's results according to prior information or physical intuition. The primary assumption used in this analysis is that all noise corruptions have stationary statistics. As a result of that assumption, all measurement weightings are chosen to be constant. No precise criteria were used for the selection of those weightings. The weightings were selected so they would physically match the measured values, within reason. Several different weighting schemes were investigated and the following method was chosen for the trajectory reconstruction.

The weightings were selected open loop in a way that high priority was given to the radar data and lower priority to the meteorological and pneumatic data. With the exception of measurements taken at very low dish elevation angles, the radar data were considered to be quite reliable; for the flight to be analyzed, range errors were believed to be within 0.6 to 2.5 m (2 to 5 ft) and velocity to within 1 m/sec (3 ft/sec). For this reason the radar measurements were used as the standard against which the relative weightings of the meteorological and pneumatic data were selected; that is, the radar components were all given a weighting of 1 and the other weights were selected relative to this value.

The meteorological data provided only a "ballpark" value for the winds and had no high-frequency content. The "goodness" of these data was contingent on the changes in weather patterns as well as the accuracy of the original meteorological observations. On the day the flight was analyzed, the general weather conditions were relatively benign; that is, the wind speeds were relatively low and the weather

pattern did not deform or move a lot in the twelve-hour period between observations. Air mass temperature changes were, however, greater than typical at altitudes of between 3657.6 and 8534.4 m (12,000 and 28,000 ft). Because of these changes, sizable shifts in wind direction and velocity were noted between those altitudes. Examples of values for the meteorological parameters, their changes during the twelve-hour period in which the flight test occurred, and subjective estimates of confidence in their values are given in table 1.

The filter estimates of the winds should follow the gross trend of the meteorological data; however, because of higher frequency atmospheric phenomena, deviations from this trend must be allowed. Weightings between 0.20 and 0.40 gave a physically reasonable match between the estimated and measured winds.

Because of the random temperature effects, the airspeed measurements (derived from the backup transducers) were considered to be less reliable than the radar measurements. Too high of a weighting of the airspeed components tended to pull the Earth-relative velocity estimates away from the radar values, while too low of a weighting tended to allow no deviations of the wind estimates from the meteorological values. Weightings between 0.15 and 0.40 gave physically satisfactory matches between the radar data and the Earth-relative velocity estimates; a weighting of 0.15 gave a nearly identical match between the estimated and meteorological winds, and a weighting of 0.40 allowed random deviations of approximately 1 m/sec (3 ft/sec) between the estimated and meteorological winds. Because a weighting of 0.40 allowed for high-frequency oscillations, it was chosen as the most physically reasonable. Table 2 presents the measurement weightings which were used.

Computation of Air Data From the Estimated States

The air data are computed from the state estimates by performing several steps outside of the filter loop. This computation procedure is presented in figure 5. The steps of this procedure are: (1) The airspeed components in the northerly, easterly, and vertical directions are computed by adding the appropriate LKF Earth-relative velocity estimates and the LKF wind velocity estimates. (2) Using the Euler angles, the direction cosine matrix is computed and the airspeed components are rotated to body axis. (3) Total airspeed and angles of attack and sideslip are computed from the airspeed components. (4) Ambient temperature and pressure are computed using the barometric model discussed in the DATA SOURCES AND INSTRUMENTATION section and the LKF estimate of geometric altitude. (5) Using ambient temperature and pressure values and LKF airspeed, the Mach number, dynamic pressure, and pressure altitude are computed.

Computation of Bias Errors in Estimates

It was determined that a method in which the bias errors in the LKF estimates may be quantitatively assessed needed to be developed. This could be accomplished by examining the innovation (residual) between the measured system response (that is, the z vector) and the predicted response of the system (that is, the vector $Cx_f(t)$). Define the vector e(t) as

$$e(t) = Z(t) - Cx_f(t)$$

The mean value of this quantity should be zero (ref. 7) and any deviation from zero is indicative of bias errors in the estimates. Since stationary statistics have

been assumed, the ergodic assumption that the sample mean of the innovation vector is a close approximation of the true mean has been made. As a result, the bias errors in the LKF estimates are approximated by

$$S(e) = \sum_{j=1}^{ND} \left[z(j) - Cx_f(j)\right] / (ND-1)$$

where ND is the number of samples chosen to give a statistically representative ergodic set. In other words, the bias errors in the LKF results have been approximated with the averages of the measurement residuals.

Using the estimated bias errors in the LKF wind-relative velocity components, and propagating these errors by use of the chain rule, an approximation of the bias error in the LKF estimate of true airspeed can be derived. This error is combined, using the chain rule, with the uncertainty in ambient temperature to result in the uncertainty in the estimate of LKF Mach number. The bias errors in the estimate of the other air data quantities are computed in a similar manner. The results of this bias error analysis are presented in the VALIDATION section.

Separation of Transducer Errors From Measurement Errors

As previously discussed, a method in which transducer measurement errors may be separated from the actual aircraft position error needed to be developed. The unique and somewhat fortunate configuration of the HiMAT air data measurement system allowed for this separation. The three key elements for separation are: (1) Referring again to figure 2(b), the static and impact pressure transducers (both main and backup) are fed by the same static pressure source and any position error will affect the indicated static and impact pressures in equal, but opposite directions. This is because impact pressure is the difference between stagnation and static pressure. (2) Any difference between the indicated pressure values (both static and impact), as measured by the main and backup transducers, will be due entirely to transducer errors. This is because the main and backup transducers are fed by the same physical pressure source. (3) The results of the error analysis (to be presented in the VALIDATION OF THE LKF TECHNIQUES section) indicate that the LKF air data estimates are highly accurate, and as a result, may be used as a close approximation of the true air data values.

The mathematical description of the error analysis is: The indicated values of static and impact pressure can have two actual error sources — an error caused by position error, and one that results from faulty transducer measurements. The errors in the indicated values of static and impact pressure because of transducer error are identified as $\delta(P)$ and $\delta(Qc)$. The errors in static and impact pressure because of position error are identified as $\Delta(P)$ and $\Delta(Qc)$. Referring to element 1 of separation:

$$\Delta(Qc) = -\Delta(P) \tag{3a}$$

and referring to element 3 of separation, the true value can be approximated by the LKF value; the relations for true static and impact pressure are

$$Qc_f = \left[Qc_i + \delta(Qc) - \Delta(P)\right] \tag{3b}$$

$$P_f = \left[P_i + \delta(P) + \Delta(P)\right] \tag{3c}$$

In a similar manner, the true value of Mach number can have two error sources: an error because of position error, $\Delta(M)$, and an error because of transducer measurement error, $\delta(M)$. This relationship is

$$M_{true} = \left[M_i + \delta(M) + \Delta(M)\right] \tag{3d}$$

However, because Mach number is a function of the ratio of impact and static pressure, equation (3d) may be equivalently expressed in terms of impact and static pressure as

$$Qc/P_{true} = \left[Qc_i + \delta(Qc) - \Delta(P)\right] / \left[P_i + \delta(P) + \Delta(P)\right]$$

Again, the LKF values replace the true values and

$$Qc/P_f = \left[Qc_i + \delta(Qc) - \Delta(P)\right] / \left[P_i + \delta(P) + \Delta(P)\right] \tag{3e}$$

Equations (3b), (3c), and (3e) are valid for both the main and backup transducer measurements; the error terms correspond accordingly. The position-error term in equations (3b) and (3c) is identical for the main and backup transducers. Referring to element 2 of separation, the differences between the main and backup indicated static pressure values and the main and backup indicated pressure values are

$$P_{i_{main}} - P_{i_{backup}} = \delta(P)_{main} - \delta(P)_{backup} \tag{3f}$$

$$Qc_{i_{main}} - Qc_{i_{backup}} = \delta(Qc)_{main} - \delta(Qc)_{backup} \tag{3g}$$

Equations (3f) and (3g) show that the differences between the values measured by the main and backup transducers are caused by transducer errors.

Equations (3b), (3c), (3d), (3f), and (3g) are used in the formulation of a system of five equations in five unknowns, thereby allowing solutions for the approximate transducer errors and the position error. Referring to equations (3b) to (3f), it is shown that the five unknowns are: (1) the error in static pressure because of transducer error for the main static transducer, $\delta(P)_{main}$; (2) the error in static pressure because of transducer error for the backup static transducer $\delta(P)_{backup}$; (3) the error in impact pressure because of transducer error for the main impact transducer, $\delta(Qc)_{main}$; (4) the error in impact pressure because of transducer error for the backup impact transducer, $\delta(Qc)_{backup}$; and (5) the error in static pressure because of position error, $\Delta(P)$. The solution to this system of equations, and proof of the solution's existence, is further discussed in appendix B.

The solution to the system of equations (3b), (3c), and (3e) is computed at each data frame, and time histories of the transducer-related error values are stored. The resulting time histories are smoothed using a third-order finite impulse response (FIR) filter (ref. 10) over a fairly local region (±100 samples) and are then added to the corresponding indicated pressure values to form a set of error-corrected indicated pressure values. The corrected pressure values are then used in conjunction with the LKF Mach number (representing the true Mach number) to compute a traditional ΔM position-error curve. This curve is discussed in the VALIDATION section.

VALIDATION OF THE LKF TECHNIQUE

The technique in which transducer measurement errors can be separated from actual aircraft errors has been developed; the verification of the method is discussed. This verification is performed in three steps: the LKF results are compared against data points resulting from a calibrated pace aircraft; the results of the error analysis are presented; and the resulting position-error curve is compared against the position-error curve obtained from calibration data after the installation of heater blankets.

Comparison to Pace Aircraft Data

LKF Mach number and altitude are compared against the main and backup air data values (corrected for position error using data obtained after installation of the heater blankets, but not corrected for tansducer error) as well as data obtained from a calibrated pace aircraft (figs. 6 and 7). Figure 6(a) presents the Mach number time history comparisons. Figure 6(b) presents the differences between the LKF and the main, backup, and pace aircraft Mach numbers. Figures 7(a) and 7(b) present analogous comparisons for altitude. The differences between the LKF and the main and backup values are sizable, while the differences between the LKF and pace data are noticeably smaller. This good agreement between the LKF and pace data lends credibility to the assumptions made in separating transducer errors from measurement errors.

Results of Error Analysis

The results of the error analysis indicate that the expected normalized (percentage) bias error in Mach number from the LKF analysis is less than 0.0075 and that the normalized bias error in altitude is less than 0.0001. These uncertainties are small. Based on these results, the assumption that the LKF values approximate the "truth" appears to be justified. The 3σ bias uncertainties in all of the LKF estimates are presented in table 3.

Presentation of Corrected Position-Error Curve

The subsonic portion of the position-error curve (Mach 0.91 was the upper limit of the data) corrected for transducer error is presented in figure 8. Also shown is the position-error curve that resulted from data derived after the installation of heater blankets. Good agreement is noted. The worst deviation in Mach number between the curves is 0.003 and the average deviation is within 0.0025. Since the LKF position-error curve was generated independently of the curve obtained after the installation of heater blankets, it is concluded that the LKF position-error curve is accurate to within at least its level of agreement with the other curve. An average scatter of 0.0025 in position error is considered to be quite good. It must be concluded that the LKF analysis is valid and sufficiently accurate.

CONCLUDING REMARKS

Much of the highly maneuverable aircraft technology (HiMAT) calibration effort was expended on flights in which the air data pressure transducers were not performing accurately. Because of low temperatures experienced during flight, the static and impact pressure measurements showed sizable, nonrepeatable deviations from the expected values. To solve this problem, the air data transducers were wrapped in heater blankets. Three additional calibration flights were performed and the new calibration data were found to be sufficiently accurate.

The data obtained from a single flight performed before the installation of the heater blankets were used to develop and verify an advanced technique that allows for the separation of transducer measurement error from aircraft position error. A linearized Kalman filter (LKF) was used to merge data from several independent sources to reconstruct an enhanced, accurate wind-relative trajectory. This trajectory, because of its high accuracy, was used to approximate the true air data values. These true values were then used in conjunction with the unique geometry of the HiMAT air data measurement system to separate the transducer errors from the aircraft position error. This separation allowed for the computation of an accurate position-error curve even in the absence of pace aircraft data and in the presence of transducer measurement errors.

The LKF technique provides an alternative method in which the position error of an aircraft may be calibrated. The method, although requiring extensive analysis, is methodical, accurate, and inexpensive. For many flight test programs a significant part of the flight effort is devoted to obtaining accurate air data measurements by performing specially designed steady-state maneuvers. Because the LKF analysis does not require special maneuvers, it could eliminate many expensive hours of flight time.

APPENDIX A — PRESENTATION OF THE LKF ALGORITHM

System Discretization

The form of the LKF state equation is

$$d/dt[x(t)] = Ax(t) + B(t)u(t) + F\eta(t) \tag{4}$$

The state equation may be integrated to give

$$x(t) = \exp(At)\, x(0) + \int_0^t \exp(Aj)\, B(j)u(j)dj + F\int_0^t \eta(j)dj \tag{5}$$

Over the integration interval from sample k to sample k + 1 there is

$$x(k+1) = \exp(ATs)\, x(k) + \int_{kTs}^{(k+1)Ts} \exp(Aj)\, B(j)u(j)dj + F\int_{kTs}^{(k+1)Ts} \eta(j)dj \tag{6}$$

where Ts is the sample interval of the measurements. Over a small sample interval, the above integrands may be simplified by introducing the approximations

$$V(k) = 1/2(B(k)u(k) + B(k+1)u(k+1))$$

$$f\eta(k) = 1/2F(n(k) + \eta(k+1))$$

and equation (6) reduces to

$$x(k+1) = \exp(ATs)\, x(k) + \int_{kTs}^{(k+1)Ts} (\exp(Aj)\, dj)V(k) + f\eta(k) \tag{7}$$

where the matrix exponentiations can be evaluated by Taylor's expansion (ref. 11).

Letting

$$\Phi(k) = \exp(ATs) \text{ and}$$

$$\Psi(k) = \int_{kTs}^{(k+1)Ts} \exp(Aj)\, dj$$

arriving at the difference equation

$$x(k+1) = \Phi x(k) + \Psi V(k) + f\eta(k) \tag{8}$$

The form of the measurement equation is

$$Z(t) = Cx(t) + G\eta(t) \tag{9}$$

The measurement equation is discretized by inspection to give the algebraic equation

$$Z(k + 1) = Cx(k + 1) + G\eta(k + 1) \tag{10}$$

and the system is discretized.

Kalman Filter Equations

As implemented for the LKF algorithm, the Kalman filter equations (refs. 6, 7, and 8) are

(1) Prediction step:

$$x_f(k + 1/k) = \Phi(k)x_f(k/k) + \Psi(k)V(k) \tag{11a}$$

$$P(k + 1/k) = \Phi(k)P(k/k)\Phi^T(k) + FF^T \tag{11b}$$

$$Z_f(k + 1/k) = Cx_f(k + 1/k) \tag{11c}$$

(2) Correction step:

$$K(k + 1) = P(k + 1/k)C^T\left[CP(k + 1/k)C^T + GG^T\right]^{-1} \tag{12a}$$

$$e(k + 1) = Z(k + 1) - Z_f(k + 1/k) \tag{12b}$$

$$x_f(k + 1/k + 1) = x_f(k + 1/k) + K(k + 1)e(k + 1) \tag{12c}$$

$$P(k + 1/k + 1) = [I - K(k + 1)C]P(k + 1/k) \tag{12d}$$

Variables with the $_f$ symbol refer to values estimated by the filter. Variables such as $Z_f(k + 1/k)$, $x_f(k + 1/k)$, and $P(k + 1/k)$ refer to estimates at sample time $k + 1$ based on measurements up to and including sample time k. The variables $Z_f(k + 1/k + 1)$, $x_f(k + 1/k + 1)$, and $P(k + 1/k + 1)$ refer to estimates at sample time $k + 1$ based on measurements up to and including sample time $K + 1$. The variable $x_f(k + 1/k + 1)$ is the Kalman filtered result.

The filter error covariances, $P(k + 1/k)$ and $P(k + 1/k + 1)$ are the filter's estimate of the theoretical covariance in $x_f(k + 1/k)$ and $x_f(k + 1/k + 1)$. These variables result from a propogation of error analysis based on the uncertainty in the initial state vector and the subsequent operations which are performed on it. $P(0/0)$, the initial value for the filter error covariance, is arrived at mostly by guesswork. A large value is usually used and the starting value is not critical. The filter will usually converge to a steady-state value for the covariance, no matter what starting value is used.

The matrix $K(k + 1)$ is referred to as the Kalman gain matrix and is used to weight the errors between the predicted system response $Z_f(k + 1/k)$, and the measured system response $Z(k + 1)$. These weighted errors are used to correct the predicted state estimate $x_f(k + 1/k)$.

APPENDIX B — METHOD FOR SEPARATING TRANSDUCER ERROR FROM AIRCRAFT POSITION ERROR

As discussed in the main text, the separation of the transducer error from aircraft position error may be accomplished by solving the system described by equations (3b), (3c), (3e), (3f), and (3g), for the five error terms — the four transducer errors and the single error caused by aircraft position error. A vector/matrix solution approach will be used. The method is as follows: Equations (3b), (3c), and (3e) are rearranged so the error terms are grouped by themselves into an error vector; that is, the rearranged equations are

$$\begin{bmatrix} Qc_f - Qc_i \\ P_f - P_i \\ \dfrac{Qc_f P_i - P_f Qc_i}{P_f} \end{bmatrix} = \begin{bmatrix} 0 & 1 & -1 \\ 1 & 0 & 1 \\ -(QC/P)_f & 1 & -\left[1 + (Qc/P)_f\right] \end{bmatrix} \begin{bmatrix} \delta(P) \\ \delta(Q_c) \\ \Delta(P) \end{bmatrix} \tag{13}$$

Equation (13) is a system of three equations in three unknowns; however, no solution can yet be extracted. This is because the matrix, which relates the error vector to the left-hand side of the equation, is only of rank two and cannot be inverted. This can be seen by subtracting the second column of the matrix from the first — the result is the third column. Equation (13) is referred to as a singular system of equations. Additional information must be added in order to solve the system.

This can be accomplished by evaluating equation (13) for both the main and backup transducer values (as previously mentioned) to give two singular systems (one for the main transducer and one for the backup transducer) of three equations in three unknowns; vectorially adding these two systems (that is, by component equations) gives a single system of three equations in five unknowns. Equations (3f) and (3g) are augmented to this system to give a nonsingular system of five equations in five unknowns. This nonsingular system is of the vector/matrix form

$$Z = C[\rho] \tag{14a}$$

Where Z, a 5 by 1 vector, is

$$Z = \begin{bmatrix} 2P_f - \left(P_{i_{main}} + P_{i_{backup}}\right) \\ 2Qc_f - \left(Qc_{i_{main}} + Qc_{i_{backup}}\right) \\ Qc_f\left(P_{i_{main}} + P_{i_{backup}}\right) - P_f\left(Qc_{i_{main}} + Qc_{i_{backup}}\right) \\ P_{i_{main}} - P_{i_{backup}} \\ Qc_{i_{main}} - Qc_{i_{backup}} \end{bmatrix} \tag{14b}$$

C, a 5 by 5 matrix, is

$$C = \begin{bmatrix} 0 & 0 & 1 & -1 & -2 \\ 1 & 1 & 0 & 0 & -2 \\ -(Qc/P)_f & -(Qc/P)_f & 1 & 1 & -2 \quad 1 + (Qc/P)_f \\ 1 & -1 & 0 & 0 & 0 \\ 0 & 0 & 1 & -1 & 0 \end{bmatrix} \tag{14c}$$

and ρ, the 5 by 1 error vector to be solved, is

$$\rho = \begin{bmatrix} \delta(P)_{main} \\ \delta(P)_{backup} \\ \delta(Qc)_{main} \\ \delta(Qc)backup \\ \Delta(P) \end{bmatrix} \tag{14d}$$

A unique solution for the error vector is guaranteed to exist only if the inverse of C exists. A necessary and sufficient condition for the existence of the inverse of C is that the determinant of C be nonzero. The determinant is evaluated by expansion by minors. The determinant expansion is

$$DET(C) = DET \begin{bmatrix} 1 & 1 & 0 & -2 \\ -Qc/P & -Qc/P & 1 & -2[1 + Qc/P] \\ 1 & -1 & 0 & 0 \\ 0 & 0 & -1 & 0 \end{bmatrix}$$

$$+ DET \begin{bmatrix} 1 & 1 & 0 & -2 \\ -Qc/P & -Qc/P & 1 & -2[1 + Qc/P] \\ 1 & -1 & 0 & 0 \\ 0 & 0 & 1 & 0 \end{bmatrix}$$

$$-2\ \mathrm{DET}\begin{bmatrix} 1 & 1 & 0 & 0 \\ -Qc/P & -Qc/P & 1 & 1 \\ 1 & -1 & 0 & 0 \\ 0 & 0 & 1 & 0 \end{bmatrix} \tag{15}$$

Expansion of each of the terms above gives

$$\mathrm{DET}(C) = -2[1 + (Qc/P)] - 2[1 + (Qc/P)] + 4(Qc/P)$$

$$- 2[1 + (Qc/P)] - 2[1 + (Qc/P)] - 4(Qc/P)$$

$$- 2(-1) + 2(1)$$

Collecting terms gives

$$\mathrm{DET}(C) = 4[1 + 2(Qc/P) \tag{16}$$

In order for DET(C) to equal zero, then

$$Qc = -(1/2)P$$

which, because of physical constraints, can never occur. It is concluded, therefore, that the solution for the error vector as specified in equation (14a) is given by

$$\rho = C^{-1}Z$$

Ames Research Center
Dryden Flight Research Facility
National Aeronautics and Space Administration
Edwards, California, December 16, 1983

REFERENCES

1. Keller, Richard G.; Pyne, Ernest L.; and Abrams, Richard: Preliminary Data Reduction Programs for the SR-71A Category II Performance and Stability Tests. AFFTC 69-3, July 1969.

2. Larson, Terry J.; and Ehernberger, L. J.: Techniques Used for Determination of Static Source Position Error of a High Altitude Supersonic Airplane. NASA TM X-3152, 1975.

3. Kempel, Robert W.: Flight Experience With a Backup Flight Control System for the HiMAT Research Vehicle. AIAA Paper 82-1541, Aug. 1982.

4. Richardson, Norman R.; and Pearson, Albin O.: Wind-Tunnel Calibrations of a Combined Pitot-Static Tube, Vane-Type Flow-Direction Transmitter and Stagnation-Temperature Element at Mach Numbers From 0.60 to 2.87. NASA TN D-122, 1959.

5. Pitman, George R., Jr., ed.: Inertial Guidance. John Wiley & Sons, Inc., 1962.

6. Meditch, J. S.: Stochastic Optimal Linear Estimation and Control. McGraw-Hill Book Co., 1969.

7. Eykhoff, Pieter: System Identification, Parameter and State Estimation. John Wiley & Sons, London, 1974.

8. LeMay, Joseph L.; and Brogan, William L.: Kalman Filtering, Eng. 88138, Lecture Notes published for UCLA Extension Short Course, Vol. I, St. Joseph Sciences, Inc. 1984.

9. Etkin, Bernard: Dynamics of Flight — Stability and Control. John Wiley & Sons, 1958.

10. D'Azzo, John J.; and Houpis, Constantine H.: Feedback Control Systems Analysis and Synthesis. McGraw-Hill Book Co., 1960.

11. Wiberg, Donald M.: State Space and Linear Systems. Schaum's Outline Series, McGraw-Hill Book Co., 1971.

TABLE 1. — METEOROLOGICAL ESTIMATES FOR THE DAY OF FLIGHT

Parameter	Geometric altitude, m (ft)	
	4572 (15,000)	7620 (25,000)
H/HP, m (ft)	260.9 (856)	416.7 (1367)
12-hr change	15.4 (50)	30.5 (100)
Confidence level	6.1 (20)	12.2 (40)
Temperature, °C (°F)	32.06 (0.2)	-7.36 (-21.7)
12-hr change	36.38 (2.6)	37.10 (3.0)
Confidence level	35.66 (2.2)	36.20 (2.5)
Wind direction and speed, deg and knots	90, 5.60 (90, 11)	5, 7.72 (5, 15)
12-hr change	75, 0.52 (75, 1)	110, 6.69 (110, 13)
Confidence level	25, 2.10 (75, 4)	30, 1.54 (30, 3)

TABLE 2. — MEASUREMENT WEIGHTINGS (GG)

Measurement	Weighting
Vns	1
Vew	1
Vv	1
VWns	0.4
VWew	0.4
VWv	0.4
Wns	0.4
Wew	0.4
Wv	0.4
H	1

TABLE 3. — ESTIMATED BIAS ERRORS IN LKF VALUES

Parameter	Normalized Bias Error
$\Delta(M)/M$	0.0075
$\Delta(VW)/VW$	0.0042
$\Delta(V)/V$	0.0036
$\Delta(W)/W$	0.3220
$\Delta(H)/H$	0.0001

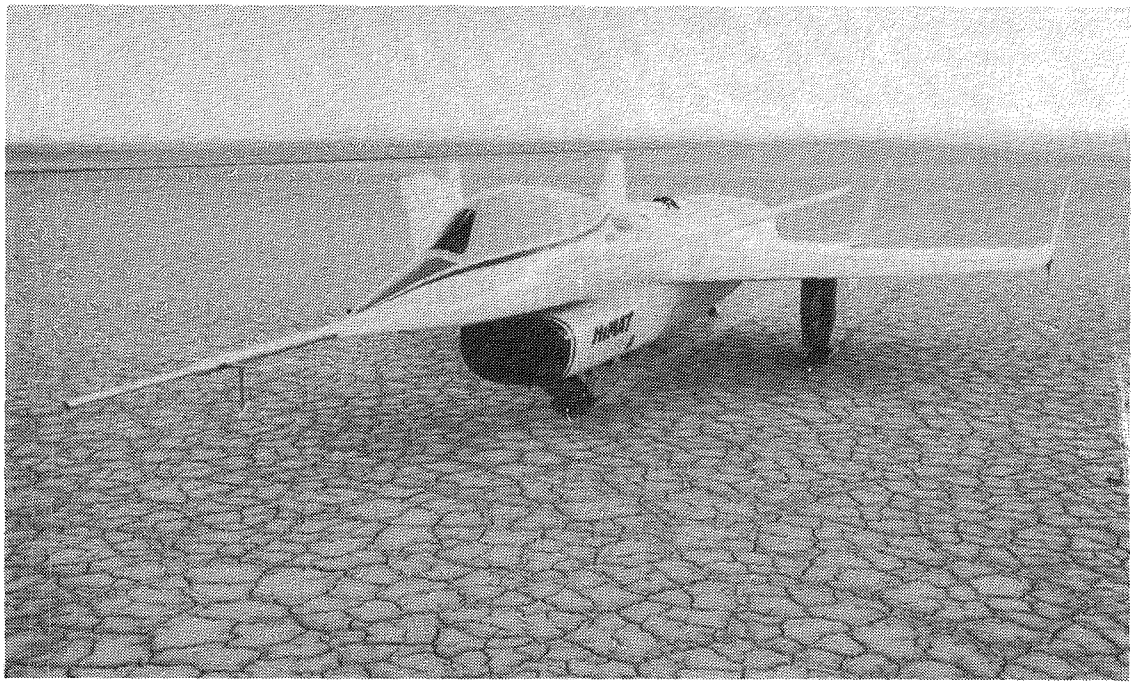

ECN 12055

(a) The HiMAT aircraft.

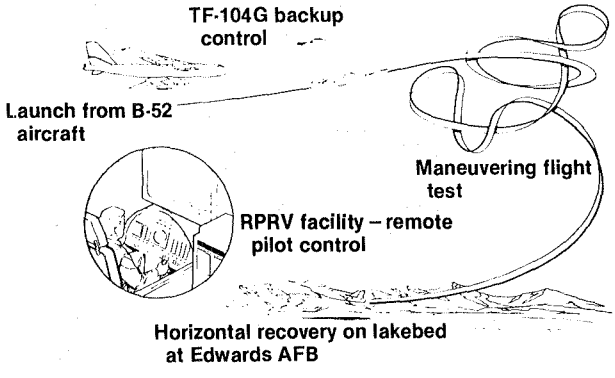

(b) The HiMAT aircraft operational concept.

Figure 1. The HiMAT aircraft and operational concept.

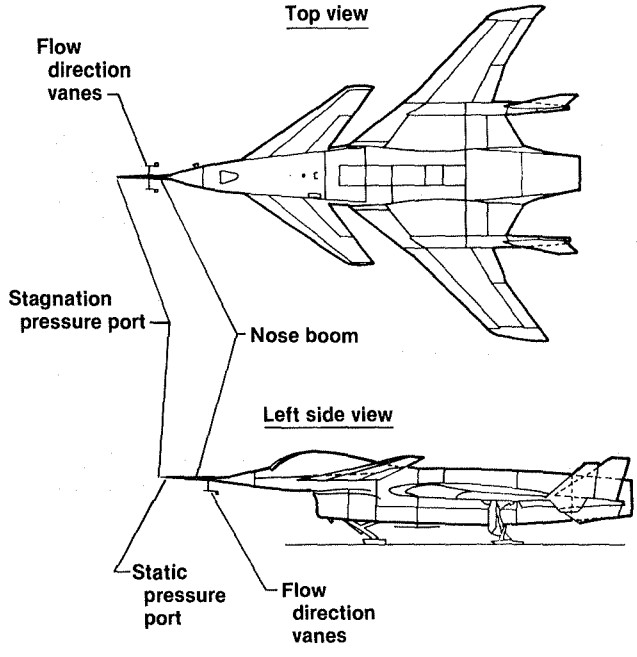

(a) Top and left side view of the HiMAT aircraft showing the noseboom.

Figure 2. The HiMAT aircraft and air data pressure measurement system.

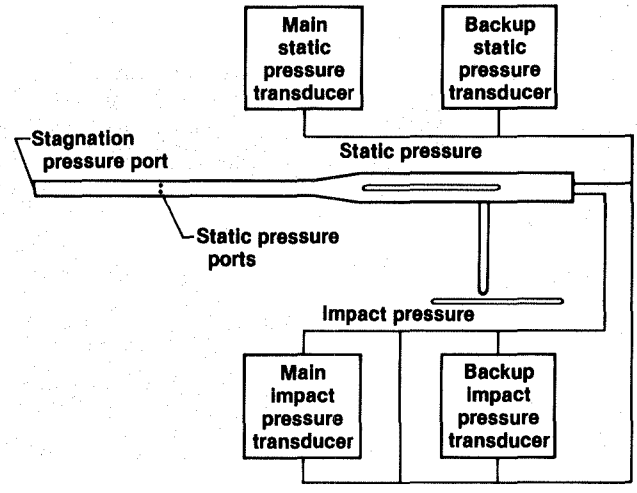

(b) Schematic of HiMAT air data pressure measurement system.

Figure 2. Concluded.

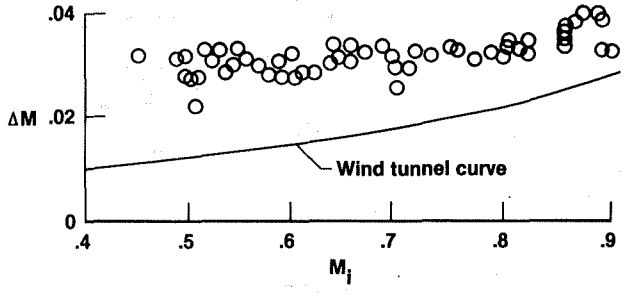

Figure 3. Position-error correction data obtained before the installation of heater blankets.

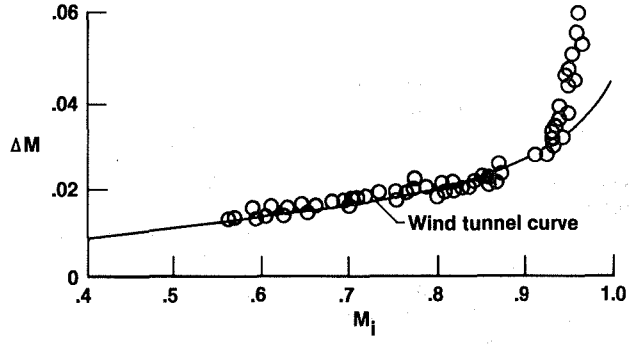

Figure 4. Position-error correction data obtained after the installation of heater blankets.

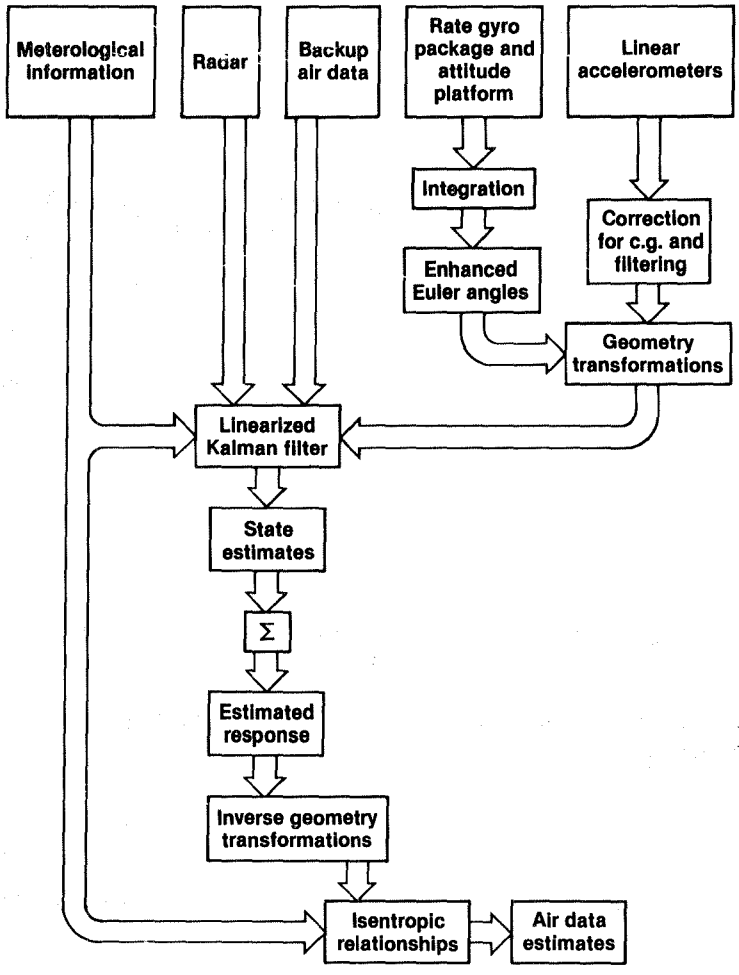

Figure 5. Flow chart of LKF computational scheme.

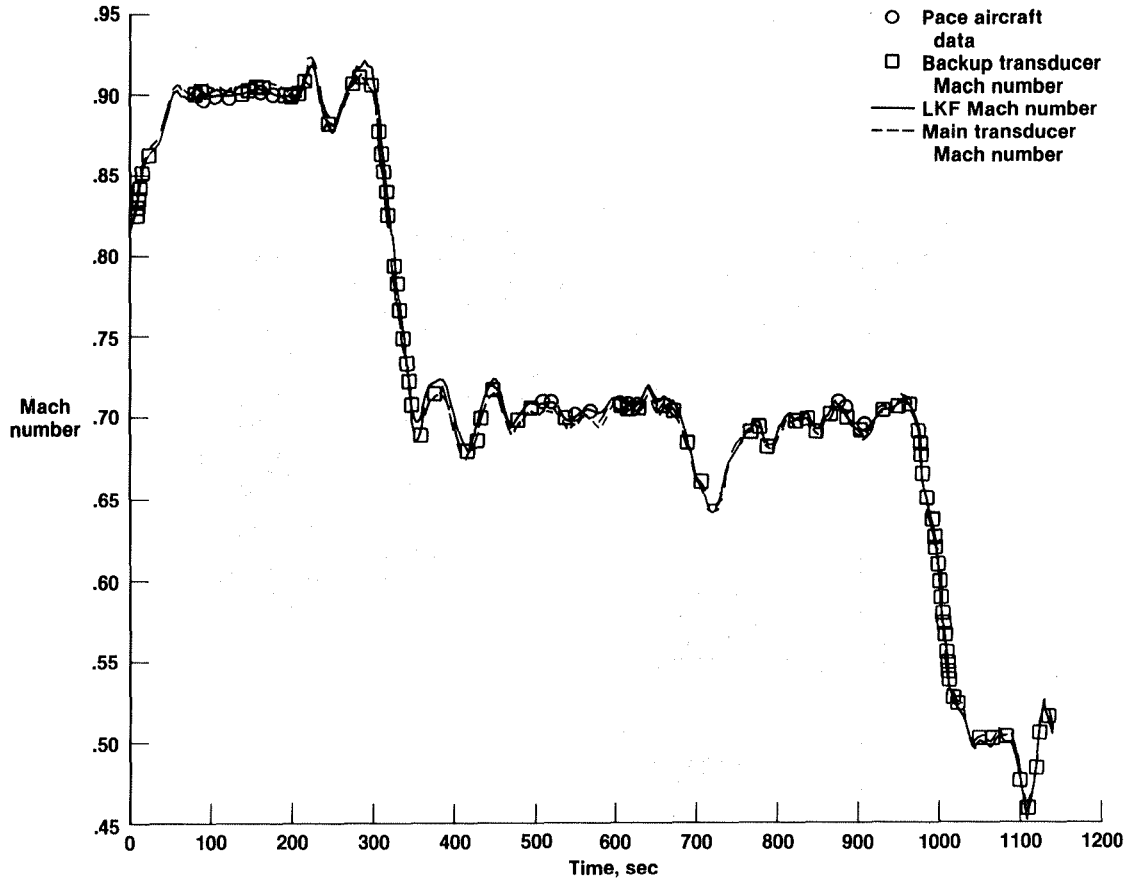

(a) Time history comparions of LKF, main, backup, and pace aircraft Mach numbers.

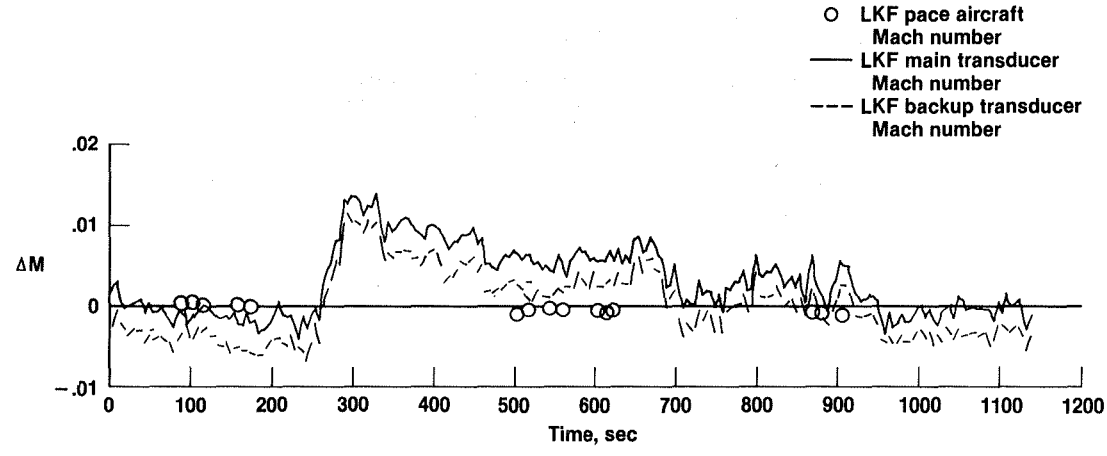

(b) Time history comparisons of differences between LKF and main, backup, and pace aircraft Mach numbers.

Figure 6. LKF Mach number validations.

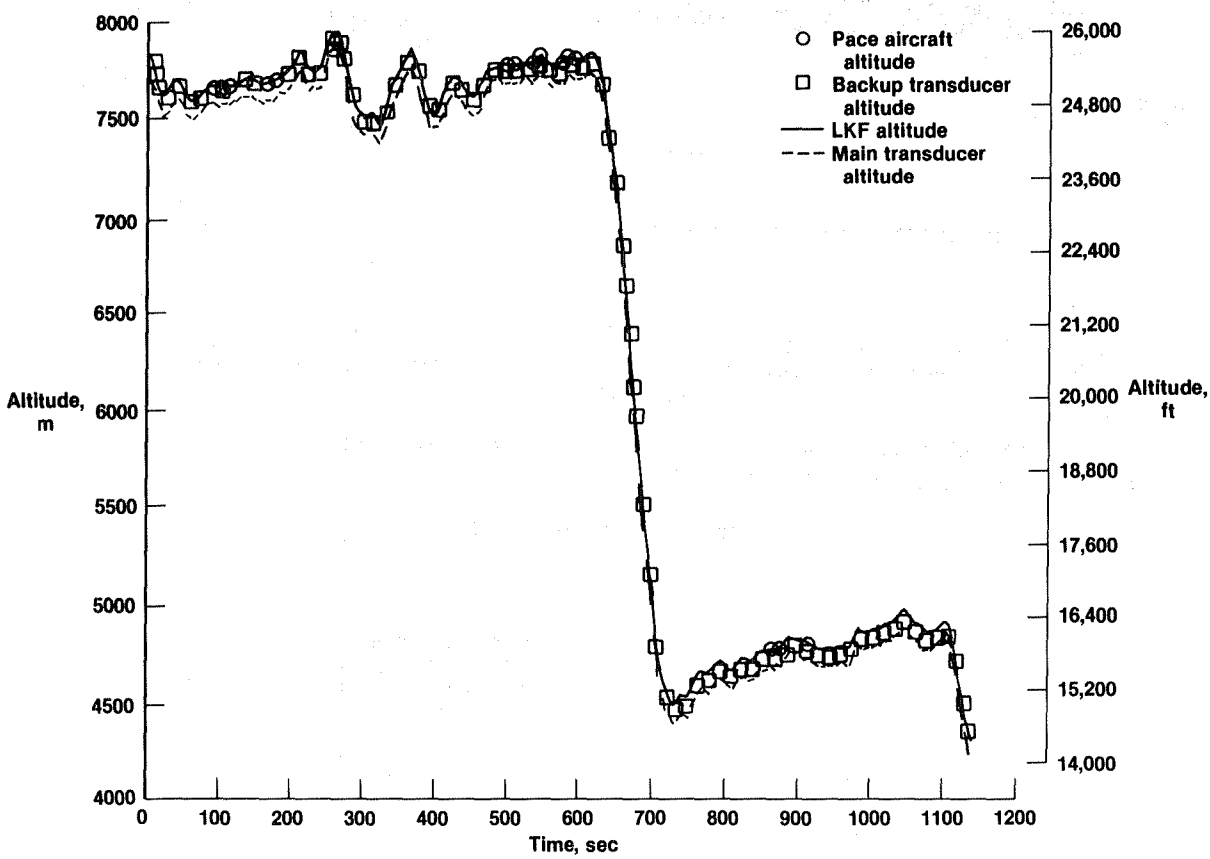

(a) Time history comparisons of LKF, main, backup, and pace aircraft altitudes.

Figure 7. LKF altitude validation.

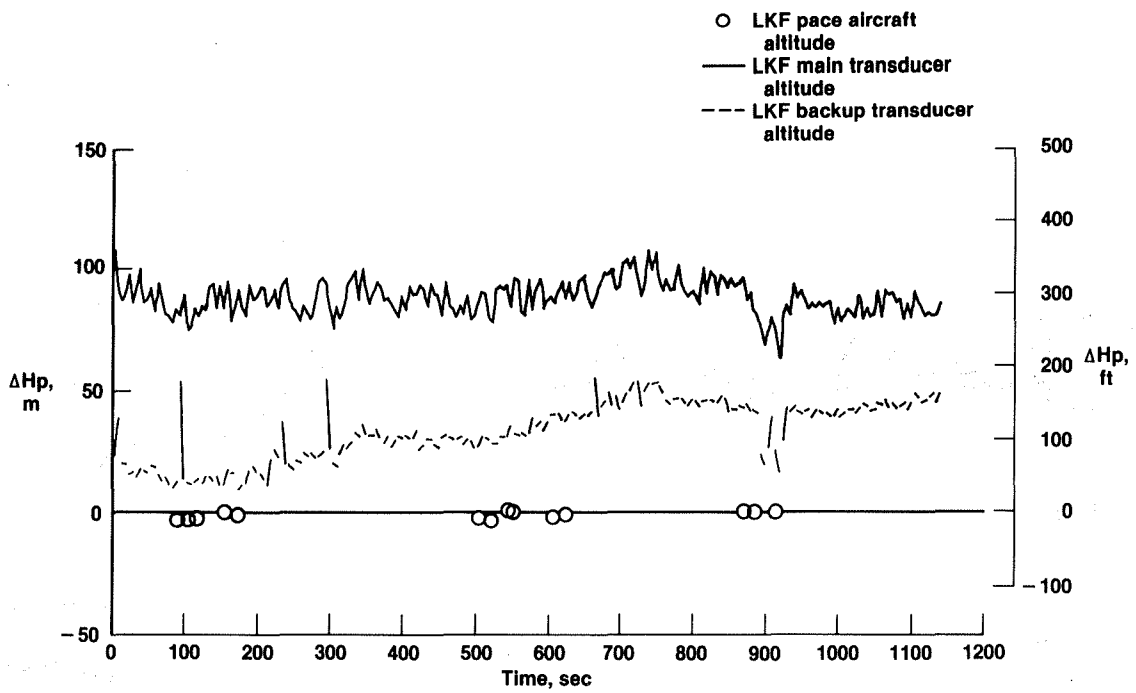

(b) Time history comparisons of differences between LKF and main, backup, and pacer aircraft altitudes.

Figure 7. Concluded.

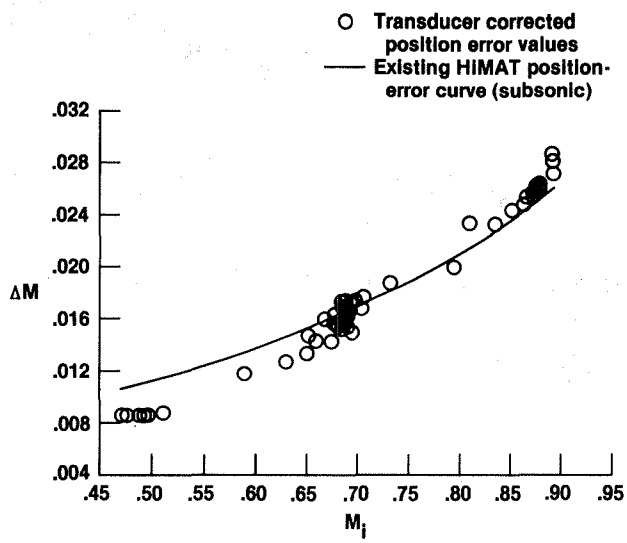

Figure 8. Comparison of corrected position error to existing HiMAT curve.

1. Report No.	2. Government Accession No.	3. Recipient's Catalog No.
NASA TM-86029		

4. Title and Subtitle	5. Report Date
Air Data Position-Error Calibration Using State Reconstruction Techniques	September 1984
	6. Performing Organization Code

7. Author(s)	8. Performing Organization Report No.
Stephen A. Whitmore, Terry J. Larson, and L. J. Ehernberger	H-1217
	10. Work Unit No.

9. Performing Organization Name and Address	11. Contract or Grant No.
NASA Ames Research Center Dryden Flight Research Facility P.O. Box 273 Edwards, California 93523	
	13. Type of Report and Period Covered
12. Sponsoring Agency Name and Address	Technical Memorandum
National Aeronautics and Space Administration Washington, D.C. 20546	14. Sponsoring Agency Code
	RTOP 505-31-21

15. Supplementary Notes

16. Abstract

During the highly maneuverable aircraft technology (HiMAT) flight test program recently completed at NASA Ames Research Center's Dryden Flight Research Facility, numerous problems were experienced in airspeed calibration. This necessitated the use of state reconstruction techniques to arrive at a position-error calibration. For the HiMAT aircraft, most of the calibration effort was expended on flights in which the air data pressure transducers were not performing accurately. Following discovery of this problem, the air data transducers of both aircraft were wrapped in heater blankets to correct the problem. Additional calibration flights were performed, and from the resulting data a satisfactory position-error calibration was obtained.

This calibration and data obtained before installation of the heater blankets were used to develop an alternate calibration method. The alternate approach took advantage of high-quality inertial data that was readily available. A linearized Kalman filter (LKF) was used to reconstruct the aircraft's wind-relative trajectory; the trajectory was then used to separate transducer measurement errors from the aircraft position error.

This calibration method is accurate and inexpensive. The LKF technique has an inherent advantage of requiring that no flight maneuvers be specially designed for airspeed calibrations. It is of particular use when the measurements of the wind-relative quantities are suspected to have transducer-related errors.

17. Key Words (Suggested by Author(s))	18. Distribution Statement
State reconstruction Air data Highly maneuverable aircraft technology (HiMAT)	Unclassified-Unlimited

19. Security Classif. (of this report)	20. Security Classif. (of this page)	21. No. of Pages	22. Price*
Unclassified	Unclassified	29	A03

*For sale by the National Technical Information Service, Springfield, Virginia 22161.

End of Document